

Article

# Reflective Semiconductor Optical Amplifier Direct Modulation Capability Enhancement Using Birefringent Fiber Loop

Zoe V. Rizou <sup>1,\*</sup> , Kyriakos E. Zoiros <sup>1</sup>, Thierry Rampone <sup>2</sup> and Ammar Sharaiha <sup>2</sup>

<sup>1</sup> Department of Electrical and Computer Engineering, Lightwave Communications Research Group, Democritus University of Thrace, GR 67 100 Xanthi, Greece; kzoiros@ee.duth.gr

<sup>2</sup> Lab-STICC UMR CNRS 6285, École Nationale d'Ingénieurs de Brest (ENIB), 29238 Brest, France; rampone@enib.fr (T.R.); sharaiha@enib.fr (A.S.)

\* Correspondence: zrizou@ee.duth.gr; Tel.: +30-25410-79-975

Received: 30 June 2020; Accepted: 27 July 2020; Published: 1 August 2020



**Abstract:** The feasibility of employing a birefringent fiber loop to enhance the performance of a directly modulated reflective semiconductor optical amplifier is experimentally demonstrated for the first time. The birefringent fiber loop acts as an optical filter of opposite slope than that of the reflective semiconductor optical amplifier electro-optical response and counteracts the finite reflective semiconductor optical amplifier modulation bandwidth of only 0.89 GHz. By proper adjustment of its detuning, the birefringent fiber loop tailors the spectral components that physically manifest due to the reflective semiconductor optical amplifier dynamic perturbation subject to direct modulation in the saturated gain regime, and suppresses the pattern-dependent distortions in the time domain. In this manner, the birefringent fiber loop manages to significantly improve the quality characteristics of the encoded signal at higher data rates than those enabled by the reflective semiconductor optical amplifier limited modulation capability. Owing to the birefringent fiber loop, the reflective semiconductor optical amplifier modulation range is extended to 4 Gb/s at the raw bit error rate of  $1.0 \times 10^{-9}$ , and to 11 Gb/s at the forward error correction limit of  $3.8 \times 10^{-3}$ . These results, which are unique against the evaluation criterion adopted in the first case, and the modulation speed achieved with post-filtering schemes in the second, highlight the beneficial role that the birefringent fiber loop can play in supporting reflective semiconductor optical amplifier operation for intensity amplification and modulation purposes.

**Keywords:** birefringent fiber loop; electrical modulation; offset filtering; pattern effect; reflective semiconductor optical amplifier

## 1. Introduction

Reflective semiconductor amplifiers (RSOAs) are special version of semiconductor optical amplifiers (SOAs) constructed with an anti-reflective coating on the front facet and a high reflectivity coating on the rear end [1]. This design modification in the active medium cavity conveniently allows an optical signal coming from one (forward) direction to have its intensity increased and at the same time its information content altered as it exits from the other (backward) direction without using additional fiber hardware and fiber connections. The RSOAs downstream amplification and upstream modulation dual functionality together with their capability of providing higher gain with lower injection currents, less polarization dependency, higher modulation linearity, lower noise figure and less temperature sensitivity than their conventional counterparts [2,3] has rendered these elements indispensable for the realization of modern access applications which critically rely on the manipulation

of bidirectionally flowing data [4–12] and where wavelength-independent, i.e., color-less, operation is highly desired [13]. Still, the data rates that RSOAs can support in these applications are limited by the RSOAs slow direct (electrical) modulation speed, which in turn is constrained by RSOAs finite modulation bandwidth being as low as very few GHz according to evidence based on experimental measurements [14] and numerical simulations [15]. A promising solution, which owing to its clear concept, feasible implementation and passive nature has gained wide popularity across the research community, is to resort to frequency discrimination and equalization [16]. The idea is to properly tailor the spectrally broadened components of the data encoded signal at the RSOA output, which occur due to the dynamic modulation of the RSOA bias current and the subsequent perturbation of the RSOA gain. For this purpose, different optical notch filtering technologies, including a delay interferometer (DI) [17,18], a fiber Bragg grating (FBG) [19], an array waveguide grating (AWG) [20] and a microring resonator [21], have been proposed. Recently, we employed a birefringent fiber loop (BFL), either alone [22], in cascade with another BFL [23] or assisted by an optical bandpass filter (OBPF) [24], to a standard SOA configured as intensity modulator. However, applying this scheme to an RSOA is not a trivial task due to the RSOA double-pass structure, which inherently imposes a greater strain on its dynamic behavior [12,25], especially subject to a fast electrical excitation [26]. Thus in this paper, we experimentally demonstrate that using a BFL can significantly boost the direct modulation capability of an RSOA. Specifically, we verify that this enhancement can be achieved well over the RSOA nominal modulation bandwidth and up to a point which can satisfy at least the mid-term needs of the target applications RSOAs are destined to serve. To this end, the BFL proven potential to improve the RSOA direct modulation performance in combination with the BFL attractive features can favor the adoption of this passive module as an efficient and affordable alternative for enabling the unobstructed exploitation of RSOAs for intensity amplification and modulation purposes.

## 2. Working Principle Qualitative Explanation

Figure 1a depicts the block diagram of the directly modulated RSOA followed by a serially connected BFL. The purpose of directly modulating the RSOA is to imprint the digital information contained in an RF signal applied to the RSOA electrical interface on an optical signal that constantly drives the RSOA. However, the faster the digital content of the RF excitation modifies the RSOA bias current, the more the data equivalent bandwidth exceeds the RSOA nominal modulation bandwidth,  $B_{mod}$ , which is finite [27], and hence the more is the process far from being ideal. As a consequence, the performance of the directly modulated RSOA becomes pattern-dependent and eventually unacceptable. Nevertheless, this performance limitation can be overcome and the RSOA be directly modulated at an extended data rate than that allowed by its limited modulation bandwidth by means of optical notch filtering. The goal pursued through the exploitation of this technique is to produce a filter characteristic which is the opposite to that of the RSOA, as shown in Figure 1b [28]. This equalizes the total frequency response and makes it independent of the electrical modulation frequency for a wider range than for the RSOA only. Moreover, by properly tailoring the frequency of occurrence of the repetitive lobes and the points of their extinction with respect to the spectral position of the encoded pulses, the spectral content of the latter can be acted upon by the filter's transmission according to their exact binary content [21,27]. In this manner, the impairments associated with these components due to the irregular RSOA gain variation by the electrical excitation are converted by the filter's slope into amplitude changes which cancel those after the RSOA [29]. Consequently, the uniformity between output pulses of same binary content and the distinction between output pulses of different binary content can be significantly enhanced. Thus the performance degradation of the encoded optical signal at the RSOA output can be sufficiently suppressed so that RSOAs can efficiently support the target applications both as external modulators and amplification elements. The desired spectral response of the compensating frequency discriminator can be technologically implemented in the polarization-based domain using a BFL, as described in the following.

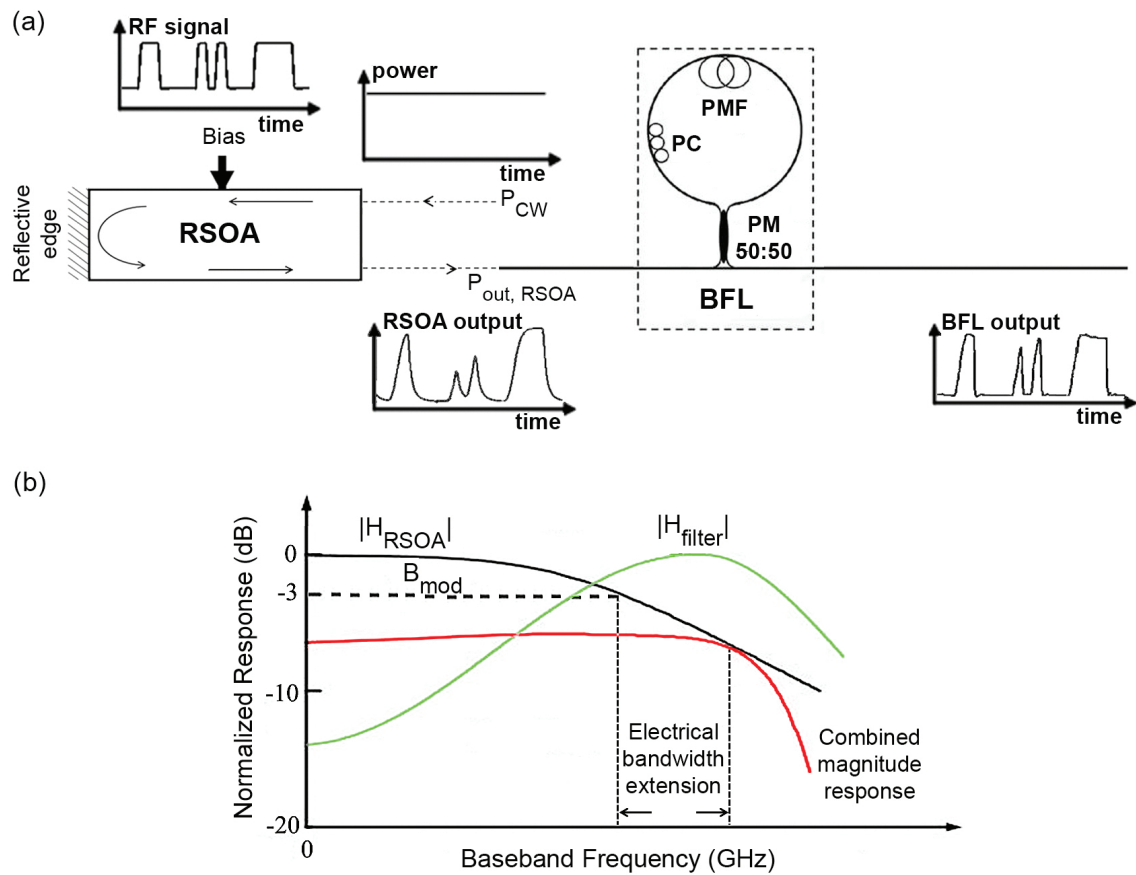


**Figure 1.** (a) Block diagram of directly modulated RSOA followed by a serially connected BFL and (b) schematic illustration of RSOA response,  $|H_{RSOA}|$ , (black line), transfer function of equalizing filter,  $|H_{filter}|$ , (green line), and combined magnitude response (red line).

### 3. Experiment

In order to run the experiments in a rational and self-consistent manner, we specified first the RSOA (CIP, model SOA-RL-OEC-1550, cf. photo in Figure 2a) driving conditions defined by the amount of the optical power and DC current, which is launched into, and biases, respectively, the RSOA.

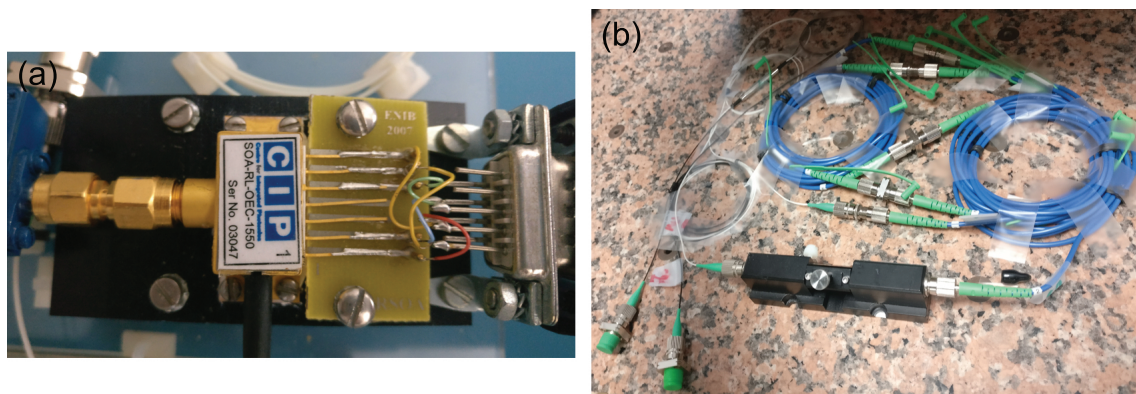


**Figure 2.** Photograph of (a) RSOA and (b) BFL modules used in the experiments.

For this purpose, we utilized as decision criterion the RSOA electrical modulation bandwidth on which we investigated the impact of these two parameters. The setup that we built to conduct the relevant measurement is depicted in Figure 3.

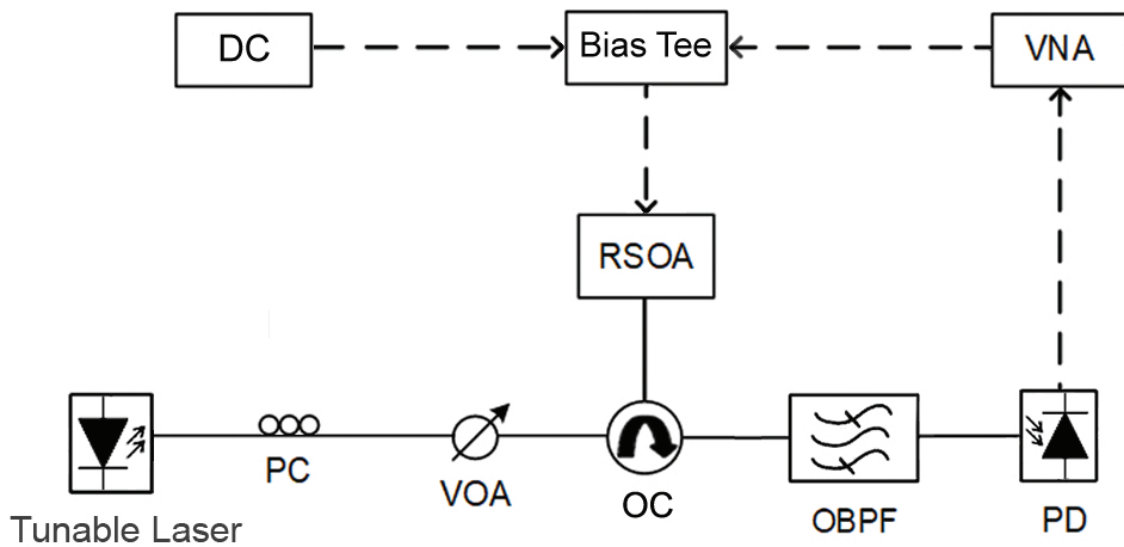


**Figure 3.** Experimental setup for measuring RSOA E/O response. RSOA: reflective semiconductor optical amplifier, VNA: vector network analyzer, OC: optical circulator, OBPF: optical bandpass filter, VOA: variable optical attenuator, PC: polarization controller, PD: photodiode. Solid and dashed lines show optical and electrical paths, respectively.

The core module was an auto-calibrated vector network analyzer (VNA). The VNA provided an RF signal that was superimposed, via a bias-tee, on the RSOA DC bias, which was thus modulated within a frequency range of 10 MHz–12 GHz for fully capturing the RSOA electro-optical (E/O) response. The variations of the RSOA gain induced due to the modulation of the injection current were mapped on a continuous wave (CW) optical signal, which was emitted from a software-controlled laser source tuned around  $\lambda = 1560$  nm and entered the RSOA through an optical circulator (OC). The RSOA encoded output was coupled back into the OC and passed through an optical bandpass filter (OBPF) to eliminate unwanted RSOA noise components. It was subsequently detected by a photodiode embedded inside the VNA and was converted again into electrical form, hence closing the circuit path established between the VNA electrical output and the VNA optical input port. In this manner, the VNA calculated the complex scattering parameter,  $S_{21}$ , and produced from its squared modulus the RSOA E/O transfer function which, as shown in Figure 4a, had a low-pass characteristic.

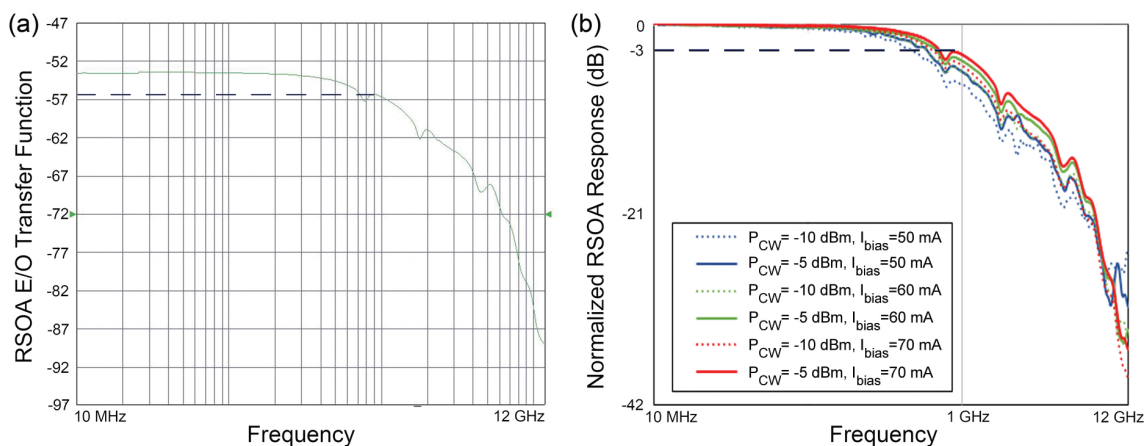


**Figure 4.** RSOA E/O response measured for (a) constant and (b) varying CW input power and DC bias. The dashed line indicates the 3-dB electrical modulation bandwidth.

By controlling the RSOA DC bias,  $I_{bias}$ , via a current source, and the CW optical power launched into the RSOA,  $P_{CW}$ , with a variable optical attenuator (VOA), we further obtained the normalized

E/O response for different values of these parameters, as shown in Figure 4b. From these curves we observed that increasing one parameter while keeping the other constant, and vice versa, was beneficial for the 3-dB electrical modulation bandwidth,  $B_{mod}$ , which in either case was increased because of the reduction of the RSOA effective carrier lifetime [30,31]. According to this evidence, choosing  $P_{CW} = -5$  dBm and  $I_{bias} = 70$  mA results in  $B_{mod, RSOA} = 0.89$  GHz. The first choice caused the RSOA gain to drop by 5.4 dB from its unsaturated value, as shown in Figure 5a.

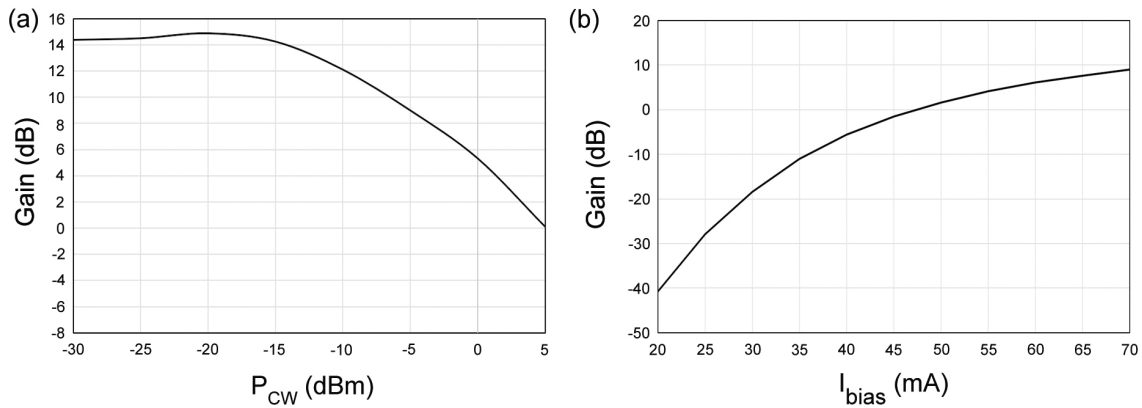


**Figure 5.** RSOA gain vs. (a) CW input power and (b) DC bias for  $I_{bias} = 70$  mA and  $P_{CW} = -5$  dBm, respectively.

Thus the RSOA was directly modulated under dynamically stressful conditions [32]. With the CW power going into the RSOA fixed to its set value, the second choice lied in the linear region of the gain-current curve shown in Figure 5b and hence made the RSOA amenable to direct modulation [33].

Having defined the RSOA operating point, the setup of Figure 3 was modified by directly modulating the RSOA with a  $2^{10} - 1$  bit-long non return-to-zero (NRZ) data from the pulse pattern generator (PPG) of a bit error rate tester (BERT) (Figure 6).

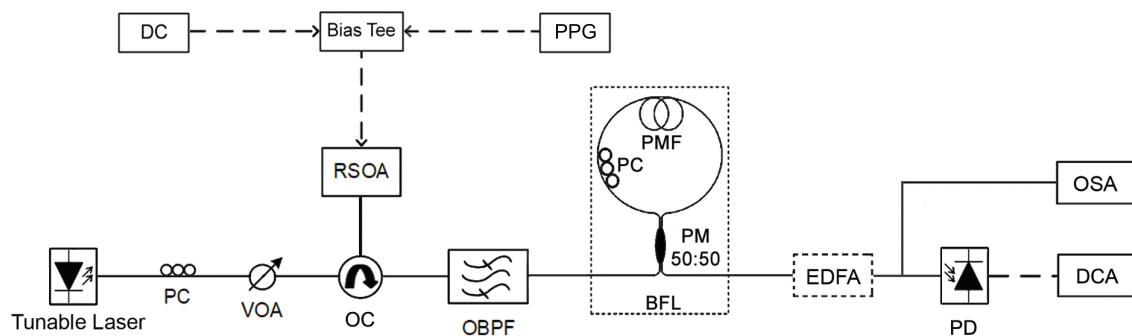


**Figure 6.** Experimental setup of RSOA electrical modulation. RSOA: reflective semiconductor optical amplifier, BFL: birefringent fiber loop, PPG: pulse pattern generator, OC: optical circulator, OBPF: optical bandpass filter, VOA: variable optical attenuator, PM 50:50: 3 dB polarization maintaining coupler, PMF: polarization maintaining fiber, PC: polarization controller, EDFA: erbium doped fiber amplifier, PD: photodiode, DCA: digital communications analyzer, OSA: optical spectrum analyzer. Solid and dashed lines show optical and electrical paths, respectively.

When this signal was applied to the  $50 \Omega$  RSOA impedance, it offset the RSOA DC current by  $\pm 10$  mA. The RSOA output was connected to a BFL (cf. photo in Figure 2b), which was implemented using a 3 dB (50:50) polarization maintaining (PM) fused coupler, an intraloop polarization controller (PC) and a segment of polarization maintaining fiber (PMF) with birefringence  $B \approx 3.3 \times 10^{-4}$  in the C-band. The total PMF length,  $L \approx 8.5$  m, resulted in the periodic comb-like transfer function shown in Figure 7a, which comprised of maxima (peaks) and minima (notches) repeated every  $\approx 0.87$  nm

(Figure 7b), equal to the BFL free spectral range ( $FSR = \lambda^2 / BL$ ). Setting the PC to generate a rotation of  $90^\circ$  to beams coming from both loop directions [34] optimized the amplitude difference between peaks and notches, or the peak-to-notch contrast ratio (PNCR), to 22 dB (Figure 7c).

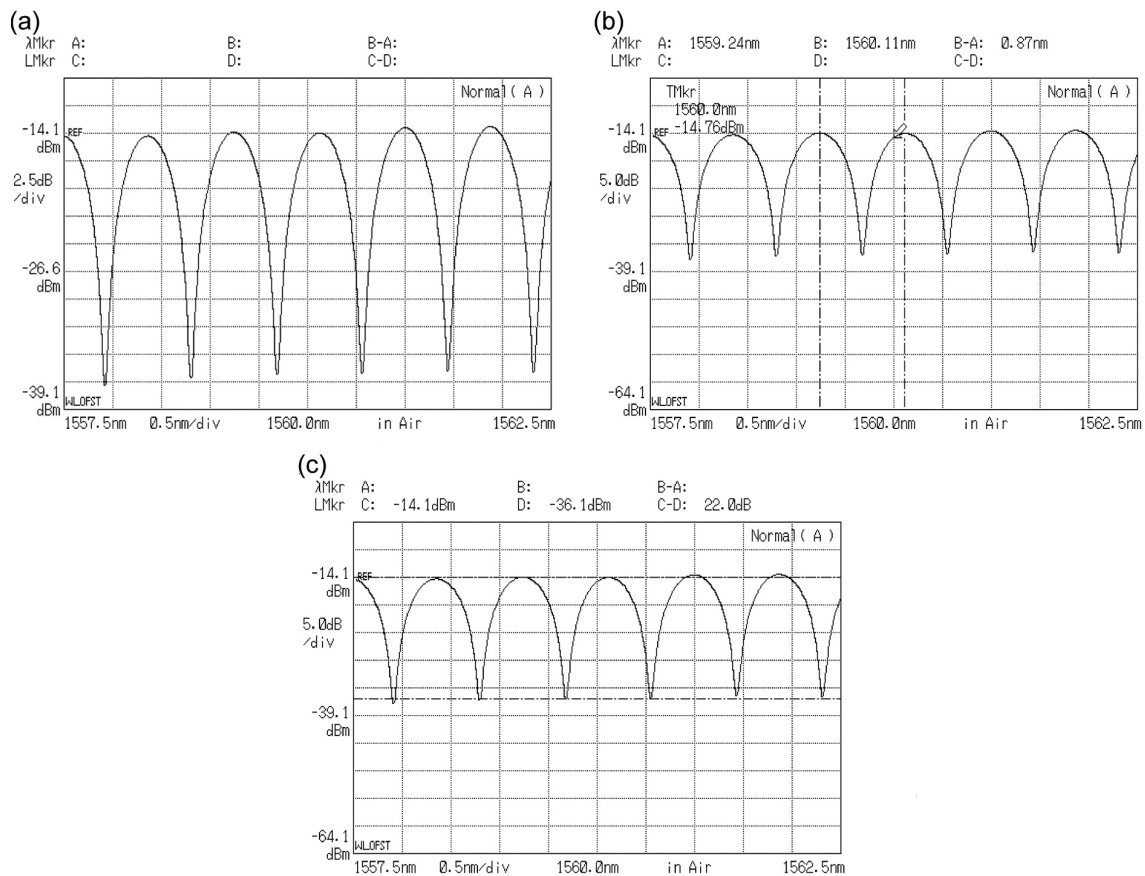


**Figure 7.** (a) BFL measured transmission response, with free spectral range (FSR) of 0.87 nm (b) and peak-to-notch contrast ratio (PNCR) of 22 dB (c) indicated by vertical and horizontal cursors, respectively.

To enhance stability against environmental perturbations by affordable means, the whole construction was enclosed inside a box, which was placed on a marbled base. In this manner, the peaks and notches could retain their spectral position without drifting for a duration that conveniently allowed taking the target measurements. In order to quantitatively assess this possibility, we observed with the help of the OSA the change in the BFL response notches' position with time. This change can be incurred due to random environmental perturbations, such as daily temperature variations or air currents from laboratory staff movements. In fact, according to a calculation conducted for the BFL and input signal parameters values in our experiment and for a typical temperature-dependent birefringence coefficient of  $-7 \times 10^{-8} / \text{K}$ , a drift in temperature of more than  $\sim 1.3^\circ \text{C}$  only can cause a notch shift beyond half the BFL FSR [35], which is the range within a notch is allowed to lie to mitigate the pattern effects induced in the RSOA [27]. Thus we found that the notches' displacement due to reasons like the aforementioned ones was of the order of  $+0.1 \text{ nm}$  for  $\sim 12 \text{ min}$ , as it can be observed in Figure 8a. This is better perceived using the experimental data derived for the notch shift in time and displaying with simulation assistance the BFL transfer function at different time instants (Figure 8b).

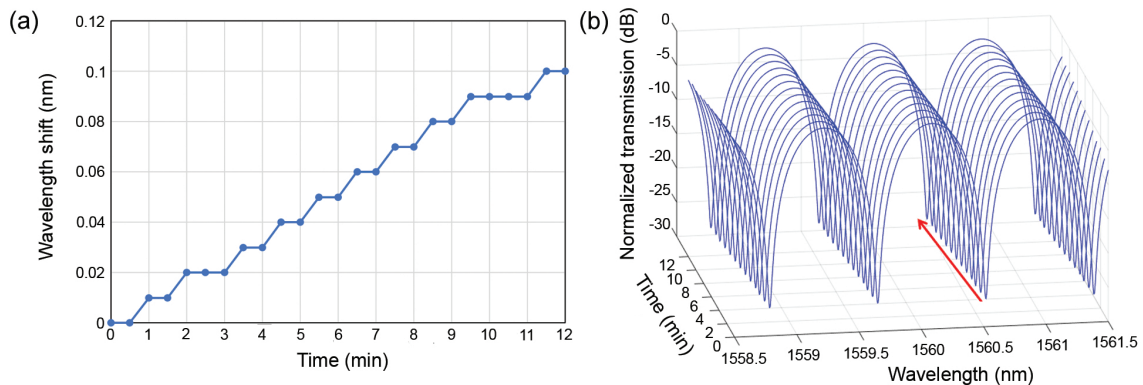


**Figure 8.** (a) BFL notch displacement vs. time, (b) BFL transfer function at different time instants. The red arrow shows the notch displacement in time.

Consequently, this interval provided enough margin to perform the experiment and obtain valid and repeatable results while scanning the relative spectral offset between carrier and notches with sufficient degree of resolution. After the permissible window closed, it was necessary to compensate for the inevitable notches' shift, and the more practical way of doing this was by fine adjusting the carrier position against the notch being closer to its longer sideband. As in our case a notch shifts with temperature at a rate of  $\sim 0.33$  nm/ $^{\circ}$ C, confining this shift to the bounds specified above would require to keep the temperature deviations within  $\pm 0.3$   $^{\circ}$ C, which in turn could be achieved with a thermoelectric cooler (TEC) [36]. The corresponding slot for measurements can be significantly extended in a more compact and flexible manner by constructing the BFL using a PM photonic crystal fiber (PCF) [35], which exhibits a notable temperature-insensitivity, in place of the conventional PMF, and an electrically, instead of manually, actuated PC with endless control of polarization [36]. Finally, the BFL was followed by a booster erbium doped fiber amplified (EDFA) to compensate for insertion losses of  $\approx 10$  dB and guarantee the same level of received power at the diagnostic equipments so as to ensure a fair comparison between measurements with and without the BFL.

#### 4. Results

Since the BFL filtering efficiency is critically determined by the detuning [23],  $\Delta\lambda$ , which is defined as the difference between the CW seeding wavelength and the wavelength of the nearest notch in the BFL response, we investigated the impact of this parameter on the operation of the scheme by assessing first the performance against the error probability (*EP*). This metric was calculated through [37]  $EP = \frac{1}{2}\text{erfc}(Q/\sqrt{2})$ , where  $\text{erfc}(x)$  is the error function and  $Q = \frac{|\mu_1 - \mu_0|}{\sigma_1 + \sigma_0}$  is the *Q*-factor, where  $\mu_{1,0}$  and  $\sigma_{1,0}$  are the mean and standard deviation of the peak power of the encoded marks ('1') and spaces ('0') whose values are extracted from the levels of the corresponding histograms. These in turn are obtained from the photodetected voltage samples that are recorded and stored by a digital communications analyzer (DCA).

The BFL detuning was practically achieved by fine tuning the CW laser wavelength relative to the adjacent notch's fixed position so that the former was spectrally located on the left-hand side of the latter. This resulted in negative detuning values and made the BFL filter transmission decrease as the wavelength increased, which is necessary [32] in order to suppress the longer-wavelength, i.e., red-shifted, spectral components induced on the encoded signal due to the self-phase modulation (SPM) effect that physically accompanies the RSOA direct modulation [38]. Equivalently, the BFL exhibited in the frequency domain a high-pass filter characteristic which counteracted that of the RSOA so that the combined response could become independent of the electrical modulation frequency for a wider range than for the RSOA only [28]. Figure 9 shows that the *EP* could be kept below  $10^{-9}$  for a RSOA direct modulation speed extended up to 4 Gb/s for  $\Delta\lambda = -0.05$  nm.

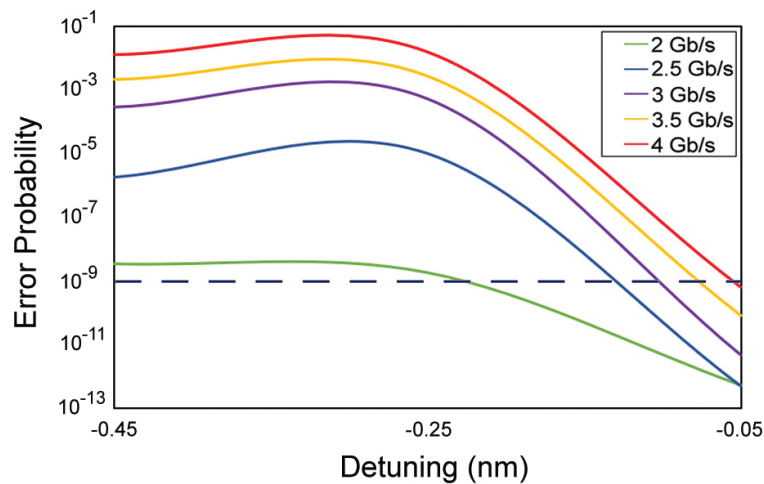


**Figure 9.** Error probability vs. BFL detuning ( $\Delta\lambda$ ) for different data rates. The dashed line indicates the limit for acceptable EP at  $1 \times 10^{-9}$ .

The feasibility of this extension was supported by Figure 10, which depicts the measured E/O response of the RSOA-BFL combination.

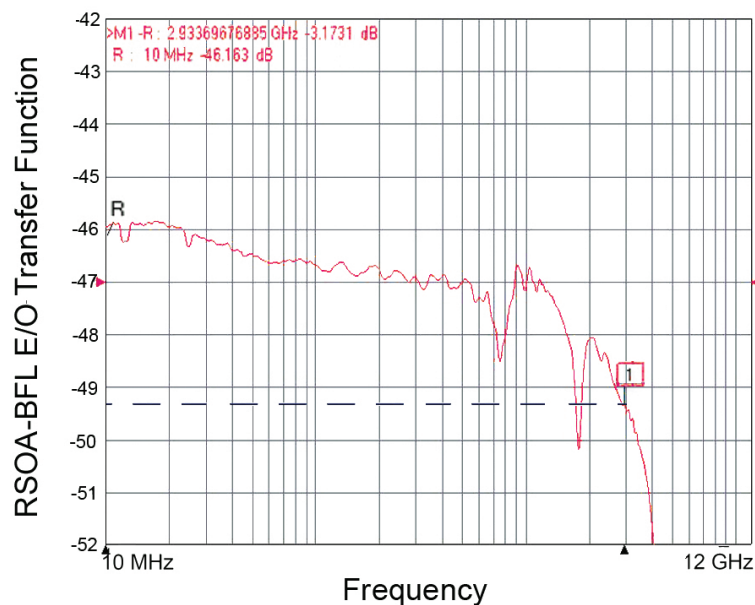


**Figure 10.** E/O response of RSOA-BFL combination. The dashed line indicates the 3-dB electrical modulation bandwidth.

It can be seen that compared to Figure 4a, the connection of the BFL after the RSOA shifted the electrical modulation bandwidth of the latter to  $\sim 3$  GHz. This value exceeded the NRZ coding pulses bandwidth, which by definition equals half the repetition data rate [39], as well as the minimum bandwidth required for optimized signal reception, which equals  $2/3$  times the data repetition rate [40]. The specified detuning value implies that the CW optical signal and BFL notch should be very closely spaced apart at the expense of very delicate experimental handling. In contrast, without the BFL, i.e., for  $\Delta\lambda = -0.45 \text{ nm} \sim FSR/2$ , it was not possible to directly modulate the RSOA at any of the checked data rates shown in Figure 9. These results were further supported by raw BER measurements obtained from the BERT error analyzer and depicted in Figure 11 for data rates between 3 Gb/s and 4 Gb/s.

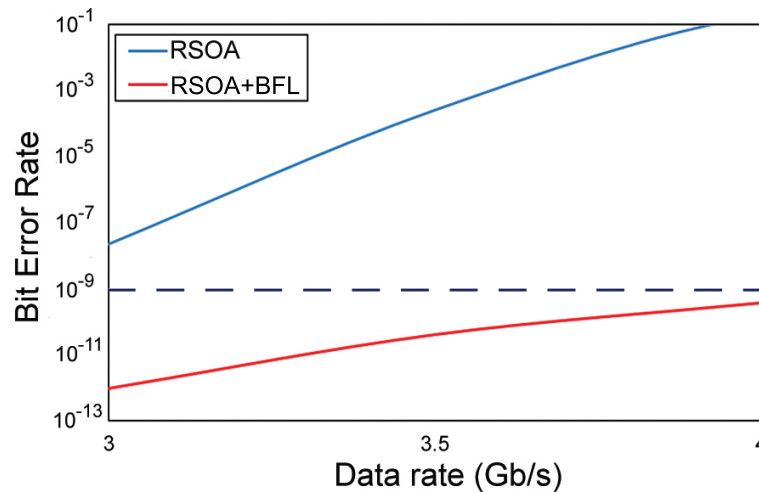


**Figure 11.** Raw BER measurements versus data rate for BFL detuning  $\Delta\lambda = -0.05$  nm. The dashed line indicates the limit for acceptable EP at  $1 \times 10^{-9}$ .

The lower bound of the displayed data rates was dictated by the fact that below 3 Gb/s, the analyzer did not find any mistakes so the measured BER was zero. In other words, the BER was so low that the analyzer needed very long time to count mistakes. Similarly, for data rates over 4 Gb/s, the analyzer had a synchronization loss since the received data could not be synchronized with the clock of the PPG. It is noteworthy that although the limit for acceptable EP,  $EP = 1 \times 10^{-9}$ , which is the standard requirement in digital communication systems [39], is several orders of magnitude tighter than that employed in other filtering schemes proposed to enable faster RSOA direct modulation by NRZ data [17–19], still the BFL managed to successfully confront this ultimate challenge. Since the RSOA nominal modulation bandwidth can be broadened by taking into account, and intervening on, factors such as the dimension [41], optical confinement [42], packaging [43], impedance matching [44] and transport effects [45] of the active device, it can be realized that there is further margin for increasing the RSOA direct modulation speed by means of the BFL. In this direction, the BFL potential was also verified in the time domain and the results are compiled and presented in Figure 12.

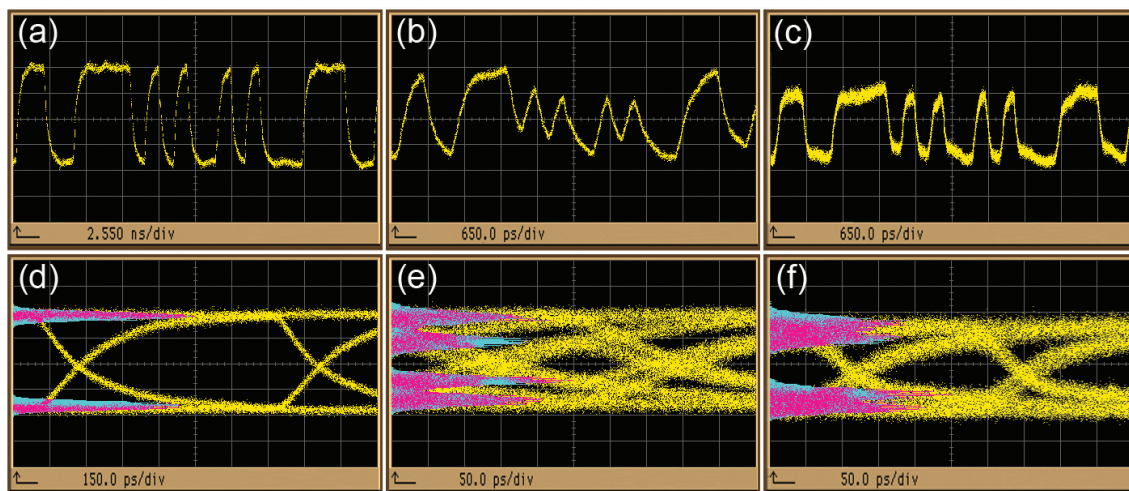


**Figure 12.** Top: Encoded pulse waveforms of (a) RSOA output at 1 Gb/s, (b) RSOA output at 4 Gb/s, (c) BFL output at 4 Gb/s for BFL detuning  $\Delta\lambda = -0.05$  nm. Bottom: Corresponding eye diagrams (d–f). Vertical scale: 15 mV/div.

These include encoded pulse waveforms for a representative 25 bit-long segment of 1100111101010010100011100 and eye diagrams for  $2^{10} - 1$  PRBS. As it can be seen, the uniformity of pulses at the RSOA output at 1 Gb/s (Figure 12a) was not preserved at 4 Gb/s (Figure 12b), since pulses

suffered from pattern-dependent peak-to-peak amplitude fluctuations. This distortion was translated into a poor quality of the eye diagram at 4 Gb/s (Figure 12e) versus 1 Gb/s (Figure 12d), as indicated by the narrow opening at the center and the dispersed histograms' content. The deteriorated outcome of the single directly modulated RSOA could be considerably improved by the properly detuned BFL, which compensated for the pulse amplitude wandering (Figure 12c) and restored the eye's opening and histograms' form (Figure 12f). These improvements were quantified by the significant reduction of the amplitude difference ( $AD$ ) of the marks [46], from the inadmissible  $AD \approx 1.55$  dB for the RSOA only, down to the more than acceptable [47]  $AD \approx 0.34$  dB thanks to the BFL, as well as by the increase of the eye opening ( $EO$ ) [39], from  $EO_{RSOA} \approx 46.68\%$  to  $EO_{BFL} \approx 70.02\%$ . Moreover, in Figure 13a it is observed that the RSOA spectrum is broadened towards the longer sideband, i.e., it is red-shifted. The spectrum retains its form at the output of the BFL at transparency, i.e., for  $\Delta\lambda = 0$  nm, since then the BFL does not act as notch filter on the red-shifted RSOA spectral components (Figure 13b). In this case, the spectrum is identical to that at the BFL input, or equivalently at the output of the OBPF right after the RSOA. In Figure 13c it can be observed instead that the corresponding spectrum becomes more symmetric at the output of the BFL, which has been detuned by  $\Delta\lambda = -0.05$  nm to suitably tailor the red-shifted spectral components.

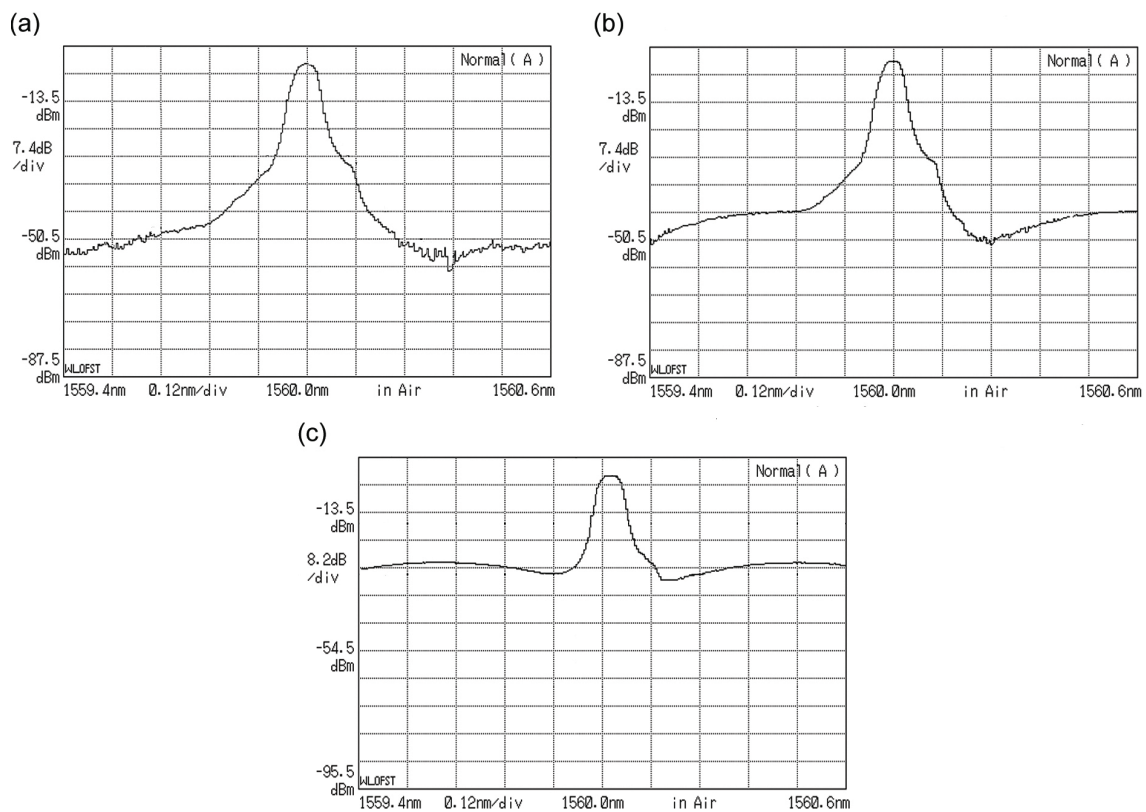


**Figure 13.** Optical spectrum at 4 Gb/s of (a) RSOA output, (b) BFL output at transparency,  $\Delta\lambda = 0$  nm, (c) BFL output for detuning  $\Delta\lambda = -0.05$  nm.

Unlike previous works, showing encoded pattern profiles and introducing appropriate indices, such as the  $AD$ , is indispensable in order to fully demonstrate and characterize the extent of distortion and amelioration undergone by the encoded signal after the stand-alone RSOA and applied notch filter (BFL in our case), respectively. To this aim, we also tested the BFL capability to allow transmission of the encoded signal over fiber. This required to specify the net gain of the RSOA and BFL combination,  $G_{net}$ , which is an important metric of the performance of post-filtering (R)SOA pattern-dependence combating [32]. This quantity is defined as  $G_{net}$  (dB) =  $G_{avg, RSOA}$  (dB) -  $G_{ar}$  (dB), where  $G_{avg, RSOA}$  is the average gain provided by the directly modulated RSOA and  $G_{ar}$  is the amplification reduction

suffered by the encoded signal due to the BFL filtering action. Therefore, the calculation of  $G_{net}$  required the knowledge of  $G_{avg, RSOA}$  and  $G_{ar}$ , which were found as follows. First, for NRZ encoding,  $G_{avg, RSOA} = G_{CW}$ , where  $G_{CW} = 8.99$  dB is the RSOA CW gain derived from Figure 5. Second,  $G_{ar}$  was extracted by measuring the mean value of the high level,  $V_{mean, 1}$ , and of the low level  $V_{mean, 0}$ , voltages, which were photodetected by the PD and recorded by the DCA, and taking their median,  $V_{med} = (V_{mean, 1} + V_{mean, 0})/2$ . This value was then compared between the BFL outputs for the case that the BFL was detuned by  $\Delta\lambda = -0.05$  nm and for the case that the BFL was detuned at transparency,  $\Delta\lambda = 0$  nm, which was equivalent to the RSOA output with BFL insertion losses compensated [32]. In this manner, we obtained  $G_{ar}$  (dB) =  $20 \log |V_{med, BFL}(\Delta\lambda = -0.05 \text{ nm}) / V_{med, BFL}(\Delta\lambda = 0 \text{ nm})| = 4.13$  dB. Therefore,  $G_{net}$  (dB) =  $8.99 - 4.13 = 4.86$  dB, which would permit propagation of the RSOA directly modulated 4 Gb/s data over approximately 20 Km of standard single-mode fiber (SSMF) without dispersion compensation. Based on this evidence, we placed an available spool of 21.35 Km SSMF after the booster EDFA, whose output power accounted for the fiber's losses. The results taken from the transmission experiment conducted under these settings showed that the form of the eye diagram was close to that when the BFL was not followed by the specific fiber spool. This is indeed verified by comparing Figure 14 to Figure 12f. Therefore the BFL could be employed in real fiber optic distribution and access fiber networks which exploit RSOAs as external modulators [1].

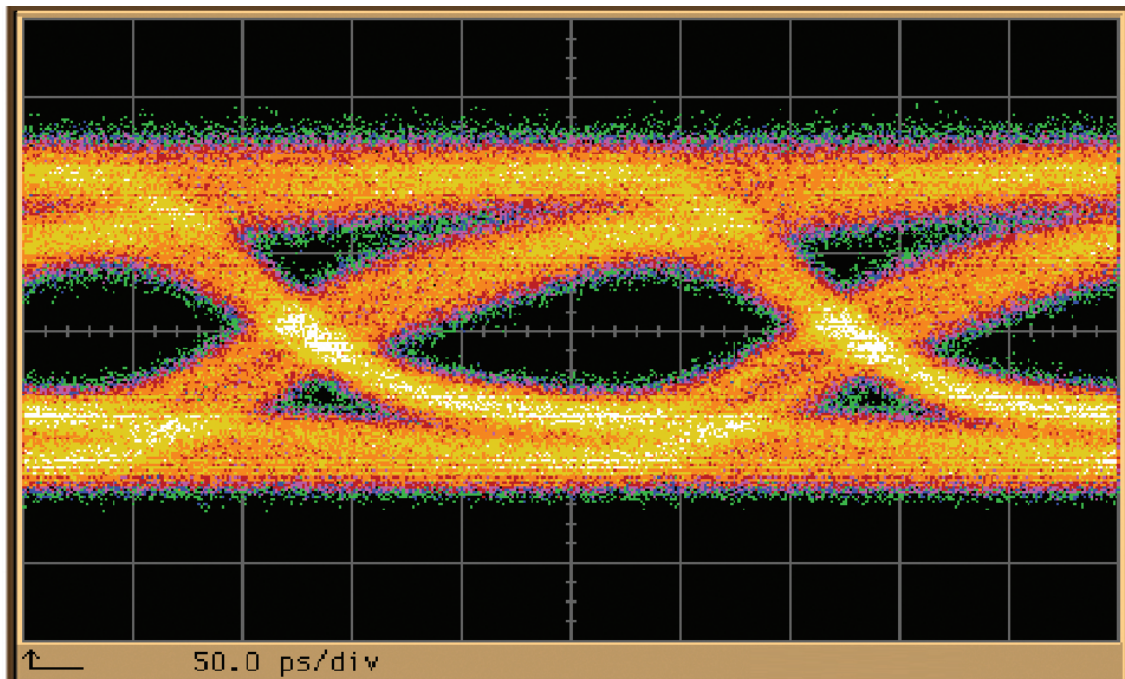


**Figure 14.** Eye diagram for 4 Gb/s encoded signal transmission over 21.35 km standard single-mode fiber after the RSOA-BFL. Vertical scale: 20 mV/div.

The previous results clearly demonstrated and confirmed that owing to the BFL it is possible to considerably increase the RSOA direct modulation speed. Given the analogous degree of extension of the nominal RSOA modulation bandwidth by other optical filtering schemes [20], we proceeded to investigate to what extent we could exploit this fact while ensuring an acceptable performance. For this purpose, we employed as evaluation criterion the  $EP$  that can be tolerated when forward error correction (FEC) is applied,  $EP_{FEC}$ . This is the metric against which the performance of directly modulated RSOAs assisted by photonic filtering schemes is commonly assessed [17–19]. Figure 15 shows that the BFL allowed  $EP_{FEC}$  to be kept below the  $3.8 \times 10^{-3}$  threshold [48] up to 11 Gb/s.

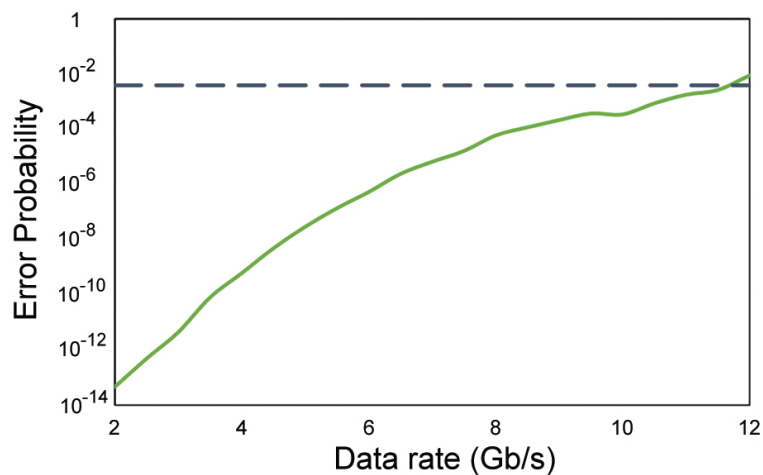


**Figure 15.** Error probability vs. data rate for BFL detuning  $\Delta\lambda = -0.05$  nm. The dashed line indicates the FEC limit at  $3.8 \times 10^{-3}$ .

This corresponds to a higher optical filter’s efficiency, which is defined as the ratio between the RSOA extended modulation speed to the RSOA modulation bandwidth, than previously reported [17–19]. Moreover, Figure 16 shows that the  $EP_{FEC}$  was minimized for an optimum detuning of  $\Delta\lambda = -0.05$  nm. This corroborates the observation and conclusion that in order to maximize the RSOA E/O bandwidth enhancement the CW signal should lie in the vicinity, and in the shorter wavelength side, of the BFL transfer function’s nearest notch. Physically this helped suppress more efficiently (Figure 17c) the spectral components of the encoded signal, which were shifted to longer wavelengths (appearing as ‘knee’ in Figure 17b) with respect to the original CW signal’s optical spectrum (Figure 17a) due to SPM inside the RSOA. To this end, the temporal profile attributes of the RSOA direct modulation outcome benefited from the properly detuned BFL, since the encoded pulse pattern form, which right after the RSOA was severely impaired (Figure 18a), was significantly improved (Figure 18b), while the corresponding eye diagram, which also suffered great distortion (Figure 18c), became open and symmetric (Figure 18d).

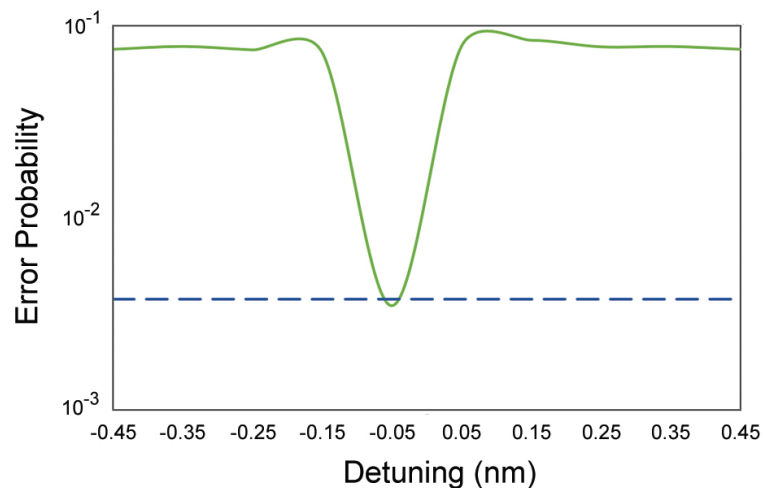


**Figure 16.** Error probability vs. BFL detuning at 11 Gb/s. The dashed line indicates the FEC limit at  $3.8 \times 10^{-3}$ .

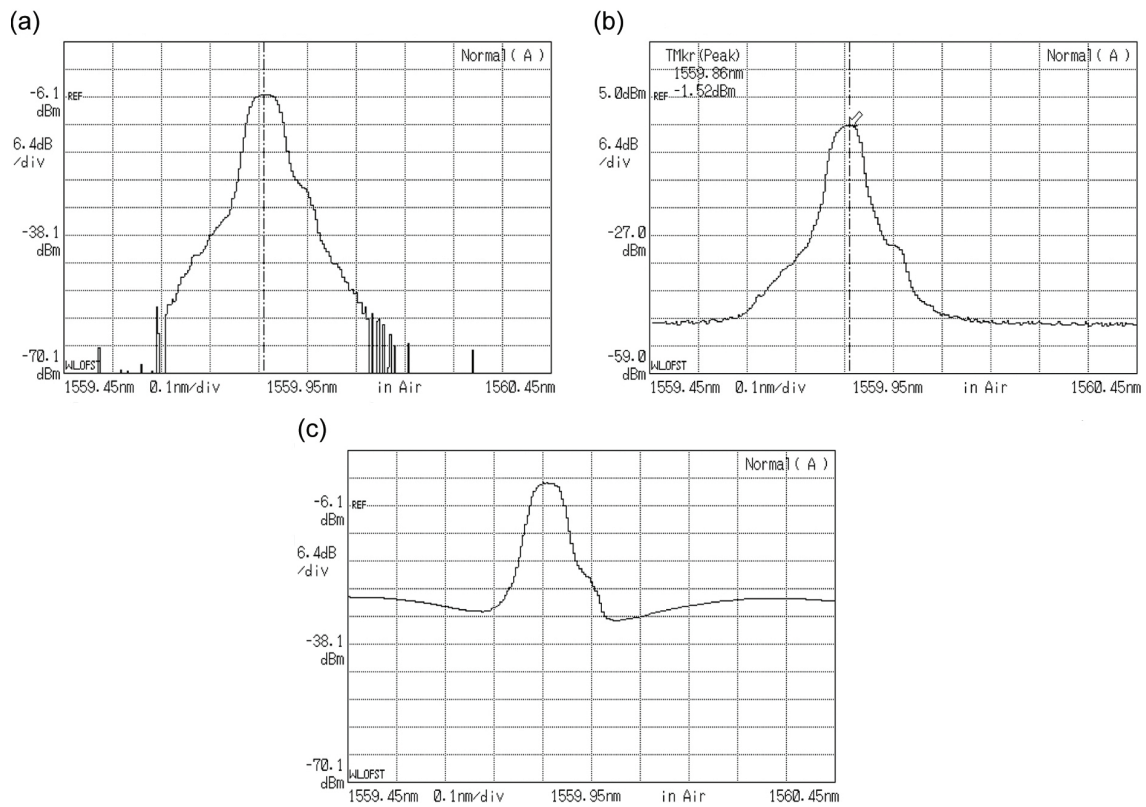


**Figure 17.** Optical spectrum at 11 Gb/s of (a) RSOA input, (b) RSOA output and (c) BFL output for detuning  $\Delta\lambda = -0.05$  nm.

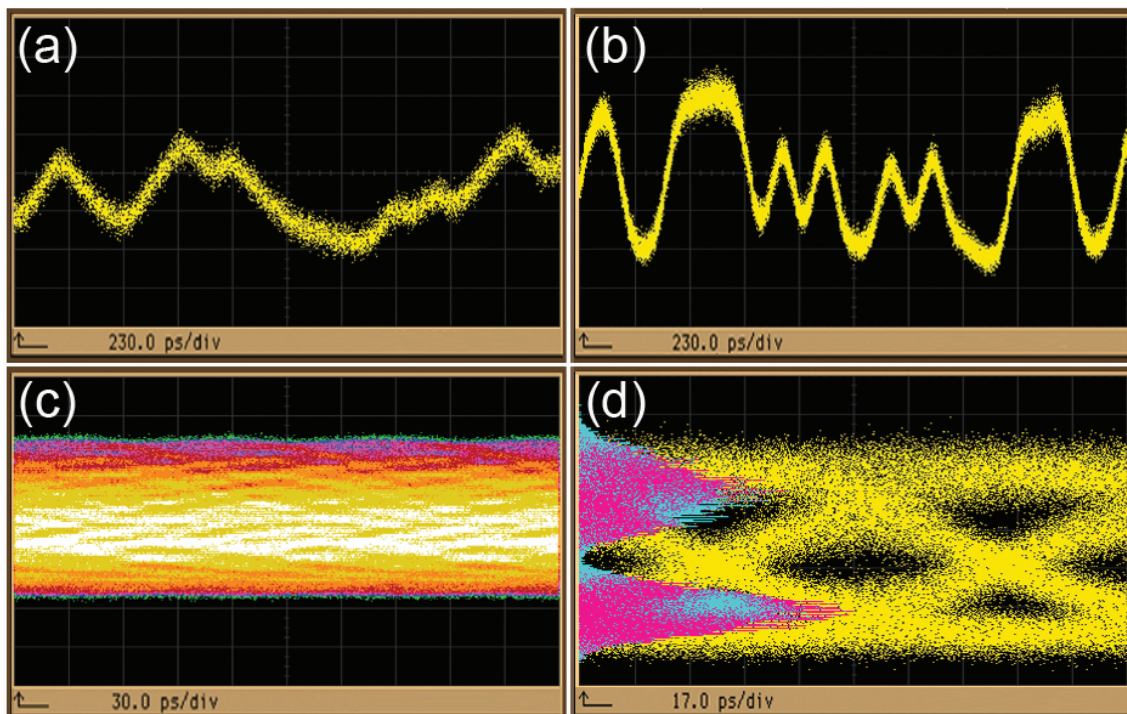


**Figure 18.** Top: Encoded pulse waveforms of (a) RSOA output and (b) BFL output for detuning  $\Delta\lambda = -0.05$  nm at 11 Gb/s. Bottom: Corresponding eye diagrams (c,d). Vertical scale: (a) 5 mV/div, (b) 15 mV/div, (c) 15 mV/div and (d) 13 mV/div.

## 5. Conclusions

In conclusion, we demonstrated through experimental work and results that a BFL can enhance the direct modulation capability of a RSOA whose modulation bandwidth is inherently limited. In this context, we showed that a properly detuned BFL allows the RSOA to produce an encoded signal of improved quality characteristics at an extended data range, which is of the order of 4 Gb/s and 11 Gb/s when the raw BER and the FEC-assisted BER is adopted as performance criterion, respectively. This fact, together with the BFL distinctive features, suggests that the BFL can constitute a viable post-filtering option for help employing RSOAs as intensity modulators in relevant applications.

**Author Contributions:** Z.V.R. conducted the experiments and interpreted the obtained results; K.E.Z. conceived the initial idea and wrote the paper; T.R. assisted the experiments, reviewed the results and the manuscript; A.S. reviewed the results and the manuscript. All authors have read and agreed to the published version of the manuscript.

**Funding:** This research received no external funding.

**Conflicts of Interest:** The authors declare no conflict of interest.

## References

1. Prat, J. *Next-Generation FTTH Passive Optical Networks*; Springer: Berlin/Heidelberg, Germany, 2008; Volume 5.
2. Connelly, M.J. Reflective semiconductor optical amplifier pulse propagation model. *IEEE Photon. Technol. Lett.* **2011**, *24*, 95–97. [[CrossRef](#)]
3. Spiekman, L.H. Active devices in passive optical networks. *J. Light. Technol.* **2013**, *31*, 488–497. [[CrossRef](#)]
4. Zhang, W.; Sun, J.; Wang, J.; Liu, L. Multiwavelength mode-locked fiber-ring laser based on reflective semiconductor optical amplifiers. *IEEE Photon. Technol. Lett.* **2007**, *19*, 1418–1420. [[CrossRef](#)]
5. Guo, L.; Connelly, M. A novel approach to all-optical wavelength conversion by utilizing a reflective semiconductor optical amplifier in a co-propagation scheme. *Opt. Commun.* **2008**, *281*, 4470–4473. [[CrossRef](#)]
6. Liu, Z.; Sadeghi, M.; de Valicourt, G.; Brenot, R.; Violas, M. Experimental validation of a reflective semiconductor optical amplifier model used as a modulator in radio over fiber systems. *IEEE Photon. Technol. Lett.* **2011**, *23*, 576–578. [[CrossRef](#)]
7. Peng, P.; Shiu, K.; Liu, W.; Chen, K.; Lu, H. A fiber-optical cable television system using a reflective semiconductor optical amplifier. *Laser Phys.* **2013**, *23*, 025106. [[CrossRef](#)]
8. Meehan, A.; Connelly, M.J. Experimental characterization and modeling of the improved low frequency response of a current modulated bulk RSOA slow light based microwave phase shifter. *Opt. Commun.* **2015**, *341*, 241–244. [[CrossRef](#)]
9. Wang, X.; Feng, X.; Zhang, P.; Wang, T.; Gao, S. Single-source bidirectional free-space optical communications using reflective SOA-based amplified modulating retro-reflection. *Opt. Commun.* **2017**, *387*, 43–47. [[CrossRef](#)]
10. Wei, H.; Krishnaswamy, S. Comparative assessment of erbium fiber ring lasers and reflective SOA linear lasers for fiber Bragg grating dynamic strain sensing. *Appl. Opt.* **2017**, *56*, 3867–3874. [[CrossRef](#)]
11. Kotb, A.; Zoiros, K.E.; Guo, C. Performance investigation of 120 Gb/s all-optical logic XOR gate using dual-reflective semiconductor optical amplifier-based scheme. *J. Comput. Electron.* **2018**, *17*, 1640–1649. [[CrossRef](#)]
12. Dúill, S.Ó.; Marazzi, L.; Parolari, P.; Brenot, R.; Koos, C.; Freude, W.; Leuthold, J. Efficient modulation cancellation using reflective SOAs. *Opt. Express* **2012**, *20*, B587–B594. [[CrossRef](#)] [[PubMed](#)]
13. Wong, E. Next-generation broadband access networks and technologies. *J. Light. Technol.* **2011**, *30*, 597–608. [[CrossRef](#)]
14. Cho, K.Y.; Takushima, Y.; Chung, Y.C. 10-Gb/s operation of RSOA for WDM PON. *IEEE Photon. Technol. Lett.* **2008**, *20*, 1533–1535. [[CrossRef](#)]
15. Totović, A.R.; Crnjanski, J.V.; Krstić, M.M.; Gvozdić, D.M. Numerical study of the small-signal modulation bandwidth of reflective and traveling-wave SOAs. *J. Light. Technol.* **2015**, *33*, 2758–2764. [[CrossRef](#)]
16. Rizou, Z.; Zoiros, K.; Connelly, M. Semiconductor optical amplifier pattern effect suppression using optical notch filtering. *J. Eng. Sci. Technol. Rev.* **2016**, *9*, 198–201. [[CrossRef](#)]

17. Kim, H. 10-Gb/s operation of RSOA using a delay interferometer. *IEEE Photon. Technol. Lett.* **2010**, *22*, 1379–1381. [[CrossRef](#)]
18. Su, T.; Zhang, M.; Chen, X.; Zhang, Z.; Liu, M.; Liu, L.; Huang, S. Improved 10-Gbps uplink transmission in WDM-PON with RSOA-based colorless ONUs and MZI-based equalizers. *Opt. Laser Technol.* **2013**, *51*, 90–97. [[CrossRef](#)]
19. Zhang, M.; Wang, D.; Cao, Z.; Chen, X.; Huang, S. Suppression of pattern dependence in 10 Gbps upstream transmission of WDM-PON with RSOA-based ONUs. *Opt. Commun.* **2013**, *308*, 248–252. [[CrossRef](#)]
20. Presi, M.; Chiuchiarelli, A.; Corsini, R.; Choudury, P.; Bottoni, F.; Giorgi, L.; Ciaramella, E. Enhanced 10 Gb/s operations of directly modulated reflective semiconductor optical amplifiers without electronic equalization. *Opt. Express* **2012**, *20*, B507–B512. [[CrossRef](#)]
21. Rizou, Z.V.; Zoiros, K.E. Theoretical analysis of directly modulated reflective semiconductor optical amplifier performance enhancement by microring resonator-based notch filtering. *Appl. Sci.* **2018**, *8*, 223. [[CrossRef](#)]
22. Zoiros, K.; Morel, P. Enhanced performance of semiconductor optical amplifier at high direct modulation speed with birefringent fiber loop. *AIP Adv.* **2014**, *4*, 077107. [[CrossRef](#)]
23. Engel, T.; Rizou, Z.V.; Zoiros, K.E.; Morel, P. Semiconductor optical amplifier direct modulation with double-stage birefringent fiber loop. *Appl. Phys. B* **2016**, *122*, 158. [[CrossRef](#)]
24. Zoiros, K.E.; Morel, P.; Hamze, M. Performance improvement of directly modulated semiconductor optical amplifier with filter-assisted birefringent fiber loop. *Microw. Opt. Technol. Lett.* **2015**, *57*, 2247–2251. [[CrossRef](#)]
25. Duill, S.O.; Barry, L.P. Improved reduced models for single-pass and reflective semiconductor optical amplifiers. *Opt. Commun.* **2015**, *334*, 170–173. [[CrossRef](#)]
26. Antonelli, C.; Mecozzi, A.; Hu, Z.; Santagiustina, M. Analytic study of the modulation response of reflective semiconductor optical amplifiers. *J. Light. Technol.* **2015**, *33*, 4367–4376. [[CrossRef](#)]
27. Rizou, Z.V.; Zoiros, K.E. Performance analysis and improvement of semiconductor optical amplifier direct modulation with assistance of microring resonator notch filter. *Opt. Quantum Electron.* **2017**, *49*, 119. [[CrossRef](#)]
28. Rizou, Z.; Zoiros, K. SOA dynamics and pattern effects. In *Handbook of Optoelectronic Device Modeling and Simulation: Fundamentals, Materials, Nanostructures, LEDs, and Amplifiers*; CRC Press: Boca Raton, FL, USA, 2017.
29. Papagiannakis, I.; Omella, M.; Klionidis, D.; Villa, J.A.L.; Birbas, A.N.; Kikidis, J.; Tomkos, I.; Prat, J. Design characteristics for a full-duplex IM/IM bidirectional transmission at 10 Gb/s using low bandwidth RSOA. *J. Light. Technol.* **2010**, *28*, 1094–1101. [[CrossRef](#)]
30. Wei, J.; Hamié, A.; Giddings, R.; Tang, J. Semiconductor optical amplifier-enabled intensity modulation of adaptively modulated optical OFDM signals in SMF-based IMDD systems. *J. Light. Technol.* **2009**, *27*, 3678–3688. [[CrossRef](#)]
31. Gebrewold, S.A. Reflective Semiconductor Optical Amplifiers (RSOAs) as Colorless Sources in Access Networks. Ph.D. Thesis, ETH Zurich, Zurich, Switzerland, 2016.
32. Rizou, Z.V.; Zoiros, K.E.; Hatziefremidis, A.; Connelly, M.J. Design analysis and performance optimization of a Lyot filter for semiconductor optical amplifier pattern effect suppression. *IEEE J. Sel. Top. Quantum Electron.* **2013**, *19*, 1–9. [[CrossRef](#)]
33. Kashany-Mizrahi, I.; Sadot, D. Low-cost adaptive directly modulated optical OFDM based on semiconductor optical amplifier. *Opt. Fiber Technol.* **2013**, *19*, 501–506. [[CrossRef](#)]
34. Zhao, Y.; Song, T.T.; Wang, Q. Recent developments and applications of polarization-maintaining fiber loop mirrors. *Instrum. Sci. Technol.* **2012**, *40*, 239–261. [[CrossRef](#)]
35. Kim, D.H.; Kang, J.U. Sagnac loop interferometer based on polarization maintaining photonic crystal fiber with reduced temperature sensitivity. *Opt. Express* **2004**, *12*, 4490–4495. [[CrossRef](#)] [[PubMed](#)]
36. Chow, C.W.; Tsang, H. Polarization-independent DPSK demodulation using a birefringent fiber loop. *IEEE Photon. Technol. Lett.* **2005**, *17*, 1313–1315. [[CrossRef](#)]
37. Johnstone, W. *Eye diagrams & BER in optical communications BER (COM) instructor manual*; OptoSci Ltd.: Glasgow, Scotland, 2010.
38. de Valicourt, G.; Pommereau, F.; Poingt, F.; Lamponi, M.; Duan, G.; Chanclou, P.; Violas, M.; Brenot, R. Chirp reduction in directly modulated multi-electrode RSOA devices in passive optical networks. *IEEE Photon. Technol. Lett.* **2010**, *22*, 1425–1427. [[CrossRef](#)]

39. Agrawal, G.P. *Fiber-Optic Communication Systems*; John Wiley & Sons: Hoboken, NJ, USA, 2012; Volume 222.
40. Säckinger, E. *Broadband Circuits for Optical Fiber Communication*; John Wiley & Sons: Hoboken, NJ, USA, 2005.
41. de Valicourt, G.; Brenot, R. 10 Gbit/s modulation of reflective SOA without any electronic processing. In Proceedings of the Optical Fiber Communication Conference, Los Angeles, CA, USA, 6–10 March 2011; p. OThT2.
42. de Valicourt, G.; Violas, M.A.; Wake, D.; van Dijk, F.; Ware, C.; Enard, A.; Make, D.; Liu, Z.; Lamponi, M.; Duan, G.H.; et al. Radio-over-fiber access network architecture based on new optimized RSOA devices with large modulation bandwidth and high linearity. *IEEE Trans. Microw. Theory* **2010**, *58*, 3248–3258. [[CrossRef](#)]
43. Cho, K.Y.; Hong, U.H.; Choi, H.; Chung, Y.C. Maximum operable speed of WDM PON employing bandwidth-limited RSOAs. *Opt. Commun.* **2014**, *312*, 159–162. [[CrossRef](#)]
44. Vacondio, F.; Sisto, M.M.; Mathlouthi, W.; Rusch, L.A.; LaRochelle, S. Electrical-to-optical conversion of OFDM 802.11 g/a signals by direct current modulation of semiconductor optical amplifiers. In Proceedings of the 2006 International Topical Meeting on Microwave Photonics, Grenoble, France, 3–6 October 2006; pp. 1–4.
45. Babić, J.P.; Totović, A.R.; Crnjanski, J.V.; Krstić, M.M.; Mašanović, M.L.; Gvozdić, D.M. Enhancement of the MQW-RSOA's small-signal modulation bandwidth by inductive peaking. *J. Light. Technol.* **2019**, *37*, 1981–1989. [[CrossRef](#)]
46. Rizou, Z.; Zoiros, K.; Houbavlis, T. Operating speed extension of SOA external modulator using microring resonator. In Proceedings of the Progress in Electromagnetics Research Symposium (PIERS), Prague, Czech Republic, 6–9 July 2015; pp. 2399–2402.
47. Vardakas, J.; Zoiros, K.E. Performance investigation of all-optical clock recovery circuit based on Fabry-Pérot filter and semiconductor optical amplifier assisted Sagnac switch. *Opt. Eng.* **2007**, *46*, 085005.
48. Hui, R.; O'Sullivan, M. *Fiber Optic Measurement Techniques*; Academic Press: Cambridge, MA, USA, 2009.



© 2020 by the authors. Licensee MDPI, Basel, Switzerland. This article is an open access article distributed under the terms and conditions of the Creative Commons Attribution (CC BY) license (<http://creativecommons.org/licenses/by/4.0/>).